

RXTE Observations of 1A 1744–361: Correlated Spectral and Timing Behavior

Sudip Bhattacharyya^{1,2}, Tod E. Strohmayer², Jean H. Swank², and Craig B. Markwardt^{1,2}

ABSTRACT

We analyze Rossi X-ray Timing Explorer (*RXTE*) Proportional Counter Array (PCA) data of the transient low mass X-ray binary (LMXB) system 1A 1744–361. We explore the X-ray intensity and spectral evolution of the source, perform timing analysis, and find that 1A 1744–361 shows ‘atoll’ behavior during the outbursts. The color-color diagram indicates that this LMXB was observed in a low intensity spectrally hard (low-hard) state and in a high intensity ‘banana’ state. The low-hard state shows a horizontal pattern in the color-color diagram, and the previously reported ‘dipper QPO’ appears only during this state. We also perform energy spectral analyses, and report the first detection of broad iron emission line and iron absorption edge from 1A 1744–361.

Subject headings: methods: data analysis — stars: neutron — techniques: miscellaneous — techniques: spectroscopic — X-rays: binaries — X-rays: individual (1A 1744–361)

1. Introduction

The transient low mass X-ray binary (LMXB) 1A 1744–361 was discovered by Ariel V in 1976, when it was in outburst (Davison et al. 1976; Carpenter et al. 1977). Since then four more outbursts have been observed from this source in the years 1989, 2003, 2004 and 2005. Bhattacharyya et al. (2006) found an unambiguous thermonuclear X-ray burst from the 2005 *RXTE* PCA data of this source, which confirmed the suggestion of Emelyanov et al. (2001) that this source harbors a neutron star. This burst also showed millisecond period brightness oscillations during the intensity rise (with the frequency ~ 530 Hz; Bhattacharyya

¹Department of Astronomy, University of Maryland at College Park, College Park, MD 20742-2421

²X-ray Astrophysics Lab, Exploration of the Universe Division, NASA’s Goddard Space Flight Center, Greenbelt, MD 20771; sudip@milkway.gsfc.nasa.gov, stroh@clarence.gsfc.nasa.gov, swank@milkway.gsfc.nasa.gov, craigm@milkway.gsfc.nasa.gov

et al. 2006), which gave the spin frequency of the neutron star (~ 530 Hz). This is because, these oscillations are produced by an asymmetric brightness pattern on the stellar surface that is modulated by rotation of the star (Strohmayer et al. 1996; Chakrabarty et al. 2003; Strohmayer & Bildsten 2006). Bhattacharyya et al. (2006) also found energy dependent dips in the 2003 PCA data, which established that this source is a dipping LMXB (dipper). Such LMXBs exhibit modulation of soft X-ray intensity with the binary orbital period (which gave the orbital period ~ 97 min of 1A 1744–361; Bhattacharyya et al. 2006). This modulation is believed to be caused by structures above the accretion disk (White & Swank 1982). This is possible only if the dippers are high inclination systems, so that the line of sight passes through these structures. Therefore, dippers provide an opportunity to constrain the properties of the upper layers of accretion disks (and the photoionized plasma above them; Jimenez-Garate et al. 2003) in LMXBs. Moreover, recently spectral lines have been discovered from several dippers, such as EXO 0748-67 (Cottam et al. 2001), XB 1916–053 (Boirin et al. 2004), X 1624–490 (Parmar et al. 2002), etc. This shows that 1A 1744–361 might be a promising source to search for these features, which could be useful to understand various X-ray emitting and absorbing components of LMXBs.

It is also important to determine the broad spectral and timing category (e.g., Z, atoll, weak LMXB, etc.; see, for example, van der Klis 2004; Kuulkers et al. 1997; Wijnands et al. 1998; Bhattacharyya 2006) of 1A 1744–361 in order to understand the nature of this source. Z sources are the most luminous LMXBs and trace ‘Z’-like curves (with three branches: horizontal, normal and flaring) in the color-color diagram. The ordinary atoll sources have luminosities in the range $\sim 0.01 - 0.2L_{\text{Edd}}$ (L_{Edd} is the Eddington luminosity), and trace ‘C’-like curves (with two branches: low intensity ‘island’ and high intensity ‘banana’; van der Klis 2004). The various portions of these curves (combined with the correlated timing features) indicate different source states (van der Klis 2004). Recently, a low intensity spectrally hard (low-hard) state has been observed from several atoll sources. Because of its horizontal branch like pattern in the color-color diagram, some authors (Muno, Remillard, & Chakrabarty 2002 (hereafter MRC); Gierliński & Done 2002) suggested that this state might be to some extent similar to the horizontal branch state of Z sources. Such a picture, if true, favors at least partial unification of Z and atoll sources. However, this horizontal branch of atoll sources occurs at a much lower luminosity, much harder spectral state, and with a much longer time scale (compared to those of Z sources; MRC), and hence we call this state ‘atoll horizontal branch’ (AHB). Here we note that AHB might actually be the known extreme island state (EIS; van der Klis 2004) of atoll sources, and detailed study of the low intensity states of the atoll sources is necessary to resolve this. We also note that there is another category of LMXBs (known as weak LMXB; luminosity $\lesssim 0.01L_{\text{Edd}}$), which comprises the faint burst sources, the low-luminosity transients (e.g., Heise et al. 1999), etc.

Many of these sources appear to be low-luminosity atoll sources (van der Klis 2004), and show timing properties similar to those of atoll sources.

In § 2, we calculate the color-color diagram, perform timing analysis, and show that 1A 1744–361 exhibits atoll behavior during outbursts. We also suggest that the previously discovered low frequency dipper QPO (Bhattacharyya et al. 2006; Jonker, van der Klis & Wijnands 1999) is connected to the low-hard state of the source. In § 3, we describe the first detection of broad iron emission line and iron absorption edge from the energy spectra of 1A 1744–361, and in § 4 we discuss our results.

2. Color-Color Diagram and Timing Analysis

The transient source 1A 1744–361 was observed with *RXTE* PCA during three outbursts. The duration (year, RXTE proposal number, RXTE observation duration) of these outbursts were ~ 2 months (2003, P80431, ~ 39 ks), ~ 20 days (2004, P90058, ~ 2 ks), and ~ 40 days (2005, P91050, ~ 15 ks). In Fig. 1, we show the light curves from the ASM and from the PCA scans of the galactic bulge (Swank & Markwardt 2001), together with the time intervals of the pointed observations with *RXTE*. Here each interval is during an outburst, and contains several observations. We note that the scans across the galactic bulge are modeled in terms of source contributions and an ellipsoidal estimate of the unresolved flux in the galactic ridge. This analysis gives a best fit to the flux of 1A 1744–361 when it is in quiescence, as well as when it is in outburst. Although, this procedure produces an estimate of the quiescent flux of the source at the level of a few tenths of a mCrab, we do not consider it a ‘positive detection’ of 1A 1744–361 in quiescence, because of systematic errors. The source was not observed with *ASCA*, *BeppoSAX*, or *XMM-Newton*. However, *Chandra* observed the field of the Ariel V error circle while 1A 1744–361 was in quiescence (Torres et al. 2004), and a faint X-ray source in this field was identified with the optical source and the radio source reported by Steeghs et al. (2004) and Rupen, Dhawan, & Mioduszewski (2003) respectively. This showed that this faint X-ray source was 1A 1744–361 in quiescence, and the very low source flux (13 counts in ~ 16 ks; Torres et al. 2004) was below the PCA detection level.

Fig. 1 shows that the first (2003) outburst was the strongest and the longest, and it had two peaks. The 2005 outburst was also strong, but the 2004 outburst was weak and provides an opportunity to understand the source in a low-hard state (see later). The pointed observations were made near the first peak of the 2003 outburst, and near the peaks of the other two outbursts. We have computed a color-color diagram (CD; Fig. 2) using the *RXTE* PCA (from only the top Xenon layers to increase signal to noise) pointed observations.

These data are from the same gain epoch (epoch 5), and hence the gains of the Proportional Counter Units (PCUs) are almost the same. This ensures minimal shifting of the source track in the CD due to the differences of the energy boundaries. The PCUs 0, 2 and 3 were on during most of these observations, and we have used the data from these PCUs to calculate most of the CD. However, for a few ObsIDs we have used data from other PCU combinations. For these ObsIDs, we choose the PCA channel ranges carefully, so that the energy boundaries are similar to those for other ObsIDs. We have defined soft and hard colors (used in the CD; Fig. 2) as the ratio of the background-subtracted counts approximately in the $(3.5 - 5.1)/(2.2 - 3.5)$ and $(8.5 - 17.8)/(5.1 - 8.5)$ keV energy bands respectively. We have also calculated a hardness-intensity diagram (HID; Fig. 2) using these data with the background-subtracted intensity in the energy range $\sim 2.2 - 17.8$ keV. These definitions are close to the definitions used by MRC, and will facilitate the comparison of our results with those of these authors. We note that we have used the ‘FTOOLS’ command ‘pcabackest’ for estimating the backgrounds, and have not included contribution due to galactic ridge emission which is in the 1° field of view of the PCA collimator. This is because the source was always $> 10 - 100$ times brighter than the galactic ridge, and hence the ridge contribution (see § 3) to the colors is not significant.

From the CD and the HID, it is clear that 1A 1744–361 was observed in two distinctly different states: a low intensity spectrally hard (low-hard) state in 2004 and a high intensity state in 2003 and 2005. In order to explore the nature of 1A 1744–361, first we have calculated the typical X-ray fluxes from this source in these two states by fitting spectra with models. The 2 – 20 keV fluxes are $\sim 4.3 \times 10^{-10}$ and $\sim 3.2 \times 10^{-9}$ ergs $\text{cm}^{-2} \text{s}^{-1}$ respectively. The peak 2 – 20 keV flux during a non-photospheric-radius-expansion thermonuclear X-ray burst from this source was 1.9×10^{-8} ergs $\text{cm}^{-2} \text{s}^{-1}$ (Bhattacharyya et al. 2006), which implies that the low intensity state luminosity $L_{\text{low}}/L_{\text{Edd}} \lesssim 0.02$ and the high intensity state luminosity $L_{\text{high}}/L_{\text{Edd}} \lesssim 0.17$. Here, L_{Edd} is the Eddington luminosity. Both of these luminosities are consistent with those of atoll sources (van der Klis 2004). Here we note that the typical luminosities of Z sources are close to the Eddington luminosity (van der Klis 2004), and hence much higher than the luminosity of 1A 1744–361.

In order to more definitively show that this source is not a Z source, next we have compared our CD (Fig. 2) with that of MRC. Fig. 1 of MRC shows that the flaring branches (FBs) of Z sources have hard colors close to 0.2 (except for GX 17+2). As the hard colors of 1A 1744–361 in the high intensity state are close to 0.3, this indicates that if this source is a Z source, it was not on the FB during the 2003 and 2005 observations. However, during the 2003 observations the source did show flares, which are not usual for the other two states (normal branch and horizontal branch) of Z sources. The hard colors of 1A 1744–361 in the low intensity state are close to 5.5 – 6. Z sources normally do not

show such high values of hard colors (see Fig. 1 of MRC). Therefore, it is not likely that 1A 1744–361 is a Z source.

Fig. 1 of MRC shows that the hard colors of atoll sources are always around or greater than 0.3 (except for GX 13+1). This, and especially the observed hard colors of the banana branches of atoll sources (see MRC) strongly indicate that 1A 1744–361 was in the banana branch during 2003 and 2005 outbursts (high intensity states; see Fig. 2). Therefore, 1A 1744–361 exhibited atoll behavior during these strong outbursts. Here we note that during the first observation of 2005 (ObsID 91050-05-01-00), the source was spectrally slightly harder and less intense (*square* symbols in Fig. 2), which might be an indication of transition between banana and island states (van der Klis 2004). We also note that this observation registers the only thermonuclear X-ray burst seen from this source (Bhattacharyya et al 2006; see also Fig. 2).

The CD (Fig. 2) shows that 1A 1744–361 traced a horizontal pattern at high hard color values in 2004. This is likely to indicate the AHB state (see § 1) of the source, because its intensity was very low, it was spectrally very hard, and it followed a horizontal track in the CD. Therefore, even during the weak outburst (in 2004), the source properties were consistent with those of atoll sources. Here we note that the small amount of observation does not allow us to determine the duration of this state. However, the time separation between the two ObsIDs (90058-04-01-00 & 90058-04-02-00) in this state was ~ 40 hrs., which may indicate that at least during this time period the source was in this low-hard state. We also note that 1A 1744–361 was not detected with hard colors in the range $\sim 0.37 – 0.5$, and it seems that the future observation of these hard colors will be indicative of the island state of the source (van der Klis 2004).

As a source state is characterized by its timing properties in addition to the position of the source on the CD, we have computed and fitted the power spectra of 1A 1744–361 (Table 1). We have found that the high frequency power spectra of all data segments are featureless, and show only white noise (but see Bhattacharyya et al. 2006 for the description of a possible kHz QPO). Therefore, for this paper we have computed and fitted the low frequency (up to ~ 100 Hz) power spectra of the data of four representative portions of the CD (Fig. 3). In these calculations we have used the event mode data from all the available PCUs, and divided the data into 250 s segments. We have constructed light curves with a bin size of 1/256 s (all the event modes have bin sizes which are submultiples of this), and then performed Fourier transforms of the time segments. An average of all these transforms from a data set gave the power spectrum. This spectrum has been binned geometrically in order to increase the signal to noise. Fig. 3 shows these spectra (from four data sets), the best fit models, and the positions of the corresponding data segments on the CD. The best

fit parameter values are given in Table 1. The power spectrum of the low intensity AHB state (2004 data) of 1A 1744–361 can be sufficiently modeled with a constant (describing the white noise) and a Lorentzian (describing the dipper QPO; Bhattacharyya et al. 2006). The centroid frequency and the rms of the Lorentzian do not significantly depend on photon energies (within error bars), which is consistent with the ‘dipper QPO’ interpretation of this feature (Jonker et al. 1999). The power spectra of all the high intensity states (2003 and 2005 data) of the source are well fitted with a constant and a power-law. The power-law describes the ‘very low frequency noise’ (VLFN; van der Klis 2004; Boirin et al. 2000; Berger, & van der Klis 1998; Agrawal & Bhattacharyya 2003), which strongly indicates that 1A 1744–361 was on the banana branch in 2003 and 2005. However, during the first observation of 2005 (ObsID 91050-05-01-00), the strength of the VLFN was significantly less than that during the other observations (at high source intensity; see Table 1 and Fig. 3). This supports the guess (made earlier in this section) that during this 2005 observation, the source was in a transition state (between banana and island; van der Klis 2004). From these timing analyses, as well as from the source luminosity and the study of the CD, we conclude that 1A 1744–361 exhibits atoll behavior during the outbursts.

3. Spectral Analysis

A CD gives an idea about the spectral evolution of the source. But to fully understand the spectral properties of 1A 1744–361, a detailed spectral analysis is essential. However, before describing such an analysis, we note that *RXTE* PCA registered excess X-ray emission from the galactic ridge during the pointed observations of the source. This is because the location of 1A 1744–361 is in the galactic ridge (galactic latitude $\approx -4^\circ.2$), and the FWHM spatial resolution of the PCA is 1° (Valinia & Marshall 1998). Therefore, we need to take this emission into account during each spectral fitting, especially if we are interested in iron features in the spectrum (as the unresolved excess emission contains an iron emission line (at ~ 6.7 keV); Koyama et al. 1986). But, the ‘pcabackest’ command (for background calculation) of ‘FTOOLS’ does not include the galactic ridge contribution (Jahoda et al. 2005). We should, therefore, model the galactic ridge spectrum at the position of 1A 1744–361 (when the source is not in outburst) and use this model (with the parameters frozen to the best fit values) in addition to the other model components to describe the source spectra.

We had one pointed observation of the source position during the source quiescence. While this observation was only about 0.9 ks in duration, we believe that the fact that it is from exactly the source position makes it preferable to sum of slews over the region. We have fitted the ‘pcabackest’ background subtracted *RXTE* PCA spectrum with the absorbed

‘Raymond-Smith’ plus power-law model ($wabs^*(raymond+powerlaw)$; Valinia & Marshall 1998). The best fit parameters are given in Table 2. We have used this model (with these best fit parameter values) as a model component for all the source spectral analyses. Next, we have chosen a high intensity source data segment (ObsID 80431-01-02-02) in order to find out typical spectral properties of 1A 1744–361 during high intensity states. We have fitted (after ‘pcabackest’ background subtraction) the corresponding spectrum with various *XSPEC* models (see Table 3). The model that gives a reasonable χ^2/dof value, contains an absorbed Comptonization (*compTT* in *XSPEC*) plus blackbody (*bbbodyrad* in *XSPEC*) as the continuum, a broad emission line (*gauss* in *XSPEC*) and an absorption edge (*edge* in *XSPEC*). Here we note that we have fixed the lower limit of the hydrogen column density (N_{H}) to $0.1 \times 10^{22} \text{ cm}^{-2}$, so that this parameter does not wander to an unphysically small value (NASA’s HEASARC nH tool gives $N_{\text{H}} \approx 0.3 \times 10^{22} \text{ cm}^{-2}$ in the source direction). We have also fixed the upper limit of the width (σ_G ; see Table 4) of the Gaussian emission line to 1.0 keV during spectral fitting (as D’ Ái et al. 2006 did), so that this line does not become unphysically broad. Moreover, as the lowest centroid energy of broad emission lines found by Asai et al. (2000) was 5.9 keV, we have chosen this energy to be the lower limit of our Gaussian line centroid energy. From Table 3, we find that both the emission line and the absorption edge of the best fit model are significantly detected (see Fig. 4). With this knowledge, we have, then, fitted the spectra of three additional data segments (one high intensity and two low intensity). Table 4 shows the best fit parameter values from these spectral analyses, as well as from the fitting of the spectrum of Table 3. The emission line and the absorption edge significantly appear in both the high intensity spectra. However, we do not find the blackbody component and the emission line in the low intensity spectra, although the absorption edge component is significantly present. The centroid energy of the emission line (~ 6 keV) and the threshold energy of the absorption edge (~ 8 keV) indicate that these are iron features (Asai et al. 2000; D’ Ái et al. 2006).

We note that, although the best fit parameters of the galactic ridge spectrum have large errors (Table 2), the detection of the iron edge features is still certain. This is because (1) the source was always $> 10 - 100$ times brighter than the galactic ridge, and (2) the galactic ridge spectrum does not have an edge component. The iron emission line from 1A 1744–361 was detected when the source was ~ 100 times brighter than the galactic ridge. Therefore, it is unlikely that the detected iron emission line originated from the ridge. Nevertheless, we have fitted the ridge spectrum with an alternative *XSPEC* model $wabs^*(bremss+gauss)$ in order to measure the strength of the iron line. We find that photons $\text{cm}^{-2} \text{ s}^{-1}$ in this line is $(1.03 \pm 0.36) \times 10^{-4}$ ($\chi^2/\text{dof} = 19.9/20$), while that in the iron emission line of the model 1 (high intensity data) of Table 4 is $(41.22^{+26.43}_{-16.67}) \times 10^{-4}$ ($\chi^2/\text{dof} = 8.9/14$). Therefore, from our results, and as the galactic ridge spectrum is separately modeled, we conclude that the

broad emission line and the absorption edge originated from 1A 1744–361.

4. Discussion

In this paper, we have reported the correlated spectral and timing behavior of the LMXB 1A 1744–361 for the first time, as well as the first discovery of iron features (broad emission line and absorption edge) in the energy spectra from this source. We have estimated the luminosity range (in the unit of Eddington luminosity) of 1A 1744–361, calculated the color-color diagram, hardness-intensity diagram and power spectra of this source, and found that 1A 1744–361 shows atoll behavior during outbursts. The source was observed at low luminosity during the weak outburst in 2004, and at high luminosity during the strong outbursts in 2003 and 2005. During the 2004 outburst, 1A 1744–361 was in the low-hard state, but there were not enough pointed observations to determine whether the source was in such a state during the rise or decay of 2003 and 2005 outbursts. Our analysis suggests that the dipper QPO (found by Bhattacharyya et al. 2006) is connected to the low-hard state (AHB; see Figs. 2 and 3) of the source. This is consistent with the finding of such a QPO from the LMXB 4U 1746–37 only during the low-hard state (Jonker et al. 2000). Also note that the dipper QPO from the LMXB EXO 0748–676 was observed during the low intensity state, but not during the high intensity state (Homan et al. 1999). The energy dependent dips of 1A 1744–361 (discovered by Bhattacharyya et al. 2006) were observed only during the high intensity states of the source (see Fig. 2). This indicates that for 1A 1744–361 the dips are correlated with the source states.

Spectral analyses show that the continuum part of the source spectra are well described by a Comptonization plus blackbody (high intensity) or by a Comptonization (low intensity). The Comptonization component might originate from an extended corona, while the origin of the blackbody might be the neutron star surface and/or the inner accretion disk (D’ Ái et al. 2006; White et al. 1986; Church & Balucińska-Church 2004). However, we note that some other model components (such as a bremsstrahlung, or a cutoff-powerlaw) instead of Comptonization also give reasonable fits for most of the cases. Nevertheless, we have used a simple Comptonization model for all our analyses, because a Comptonization component was likely to be present in the spectrum (D’ Ái et al. 2006), and with the first discovery of a broad emission line and an absorption edge in the 1A 1744–361 spectra, we have primarily focused on these features.

The threshold energies of the absorption edge are within the range 7 – 9 keV (Table 4), and hence are consistent with those expected from ionized iron (D’ Ái et al. 2006). The emission line is broad, and such broad iron lines (near 6 keV) are observed from many

LMXBs, including dippers (Asai et al. 2000). These lines may be broadened by either Doppler effects due to Keplerian motion in the inner accretion disk, or Compton scattering in disk corona (Asai et al. 2000). Analysis of high resolution spectra can likely determine the source of this broadening by measuring the detailed structure of these lines. If the Doppler effect is determined to be the real cause, then the shapes and widths of these lines may be used to constrain the inner edge radius of the disk, as well as the Keplerian speed at that radius. The former can give an upper limit of the neutron star radius (as the disk inner edge radius must be greater than or equal to the stellar radius), while both quantities may be utilized to constrain the stellar mass. Note that the constraints on neutron star mass and radius can be useful to understand the nature of the high density cold matter at the stellar core, which is a fundamental problem of physics (e.g., Lattimer & Prakash 2001; Bhattacharyya et al. 2005). The centroid energy of the broad iron emission line observed from 1A 1744–361 is less than 6.4 keV, which could be due to unresolved iron absorption lines near ~ 7 keV (Parmar et al. 2002). This suggests that 1A 1744–361 might show spectral absorption lines when observed with higher spectral resolution missions (e.g., *Chandra*, *XMM-Newton* and *Suzaku*).

This work was supported in part by NASA Guest Investigator grants.

REFERENCES

Agrawal, V. K., & Bhattacharyya, S. 2003, A&A, 398, 223.

Asai, K., Dotani, T., Nagase, F., & Mitsuda, K. 2000, ApJSS, 131, 571.

Berger, M., & van der Klis, M. 1998, A&A, 340, 143.

Bhattacharyya, S. 2006 (astro-ph/0605510).

Bhattacharyya, S., Strohmayer, T. E., Markwardt, C. B., & Swank, J. H. 2006, ApJ, 639, L31.

Bhattacharyya, S., Strohmayer, T. E., Miller, M. C., & Markwardt, C. B. 2005, ApJ, 619, 483.

Boirin, L., Barret, D., Olive, J. F., Bloser, P. F., & Grindlay, J. E. 2000, A&A, 361, 121.

Boirin, L., Parmar, A. N., Barret, D., Paltani, S., & Grindlay, J. E. 2004, A&A, 418, 1061.

Carpenter, G. F., Eyles, C. J., Skinner, G. K., Wilson, A. M., & Willmore, A. P. 1977, MNRAS, 179, 27p.

Chakrabarty, D. et al. 2003, Nature, 424, 42.

Church, M. J., & Balucińska-Church, M. 2004, MNRAS, 348, 955.

Cottam, J., Kahn, S. M., Brinkman, A. C., den Herder, J. W., & Erd, C. 2001, A&A, 365, L277.

D' Ai et al. 2006, A&A, 448, 817.

Davison, P., Burnell, J., Ives, J., Wilson, A., & Carpenter, G. 1976, IAUC, 2925.

Emelyanov, A. N., Aref'ev, V. A., Churazov, E. M., Gilfanov, M. R., & Sunyaev, R. A. 2001, Astronomy Letters, 27, 781.

Gierliński, M. & Done, C. 2002, MNRAS, 331, L47.

Heise, J. et al. 1999, ApL&C, 38, 297.

Homan, J., Jonker, P. G., Wijnands, R., van der Klis, M., & van Paradijs, J. 1999, ApJ, 516, L91.

Jahoda, K. et al. 2006, ApJS, 163, 401.

Jimenez-Garate, M. A., Schulz, N. S., & Marshall, H. L. 2003, ApJ, 590, 432.

Jonker, P. G. et al. 2000, ApJ, 531, 453.

Jonker, P. G., van der Klis, M., & Wijnands, R. 1999, ApJ, 511, L41.

Koyama, K., Makishima, K., Tanaka, Y., & Tsunemi, H. 1986, PASJ, 38, 121.

Kuulkers, E., van der Klis, M., Oosterbroek, T., van Paradijs, J., & Lewin, W.H.G. 1997, MNRAS, 287, 495.

Lattimer, J. M., & Prakash, M. 2001, ApJ, 550, 426.

Muno, M. P., Remillard, R. A., & Chakrabarty, D. 2002, ApJ, 568, L35 (MRC).

Parmar, A. N., Oosterbroek, T., Boirin, L., & Lumb, D. 2002, A&A, 386, 910.

Rupen, M. P., Dhawan, V., & Mioduszewski, A. J. 2003, ATel, 210.

Steeghs, D., Torres, M. A. P., McClintock, J. E., Garcia, M. R., & Mallen-Ornelas, G. 2004, ATel, 267.

Strohmayer, T. E., & Bildsten, L. 2006, in *Compact stellar X-ray Sources*, Eds. W.H.G. Lewin and M. van der Klis, (Cambridge University Press: Cambridge), (astro-ph/0301544).

Strohmayer, T. E., et al. 1996, ApJ, 469, L9.

Swank, J. H., & Markwardt, C. B. 2001, in *New Century of X-ray Astronomy, ASP Conference Proceedings*, Eds. H. Inoue and H. Kunieda, (San Francisco: Astronomical Society of the Pacific), 251, 94.

Torres, M. A. P., McClintock, J. E., Garcia, M. R., & Murray, S. S. 2004, ATel, 238.

Valinia, A., & Marshall, F. E. 1998, ApJ, 505, 134.

van der Klis, M. 2004, in *Compact stellar X-ray Sources*, Eds. W.H.G. Lewin and M. van der Klis, (Cambridge University Press: Cambridge), (astro-ph/0410551).

Wijnands, R. et al. 1998, ApJ, 493, L87.

White, N. E. et al. 1986, MNRAS, 218, 129.

White, N. E., & Swank, J. H. 1982, ApJ, 253, L61.

Table 1. Best fit parameters^a (with 1σ error) for the low frequency (up to ~ 100 Hz) *RXTE* power spectra from 1A 1744–361.

Reference panel no. ^b	PLN ν ^c	PLN rms ^d (%)	L_{f_0} ^e (Hz)	L_{λ} ^f (Hz)	L_{rms} ^g (%)	χ^2/dof
1	–	–	2.43 ± 0.13	2.68 ± 0.42	13.1 ± 0.7	22.51/18
2	-1.50 ± 0.21	2.0 ± 1.3	–	–	–	28.66/30
3	-1.00 ± 0.03	6.7 ± 0.2	–	–	–	23.26/30
4	-0.94 ± 0.02	6.5 ± 0.2	–	–	–	25.60/24

^aPower spectra are fitted either by constant+Lorentzian, or by constant+powerlaw in the energy range $\sim 2.6 - 30$ keV.

^bNo. of the panel in Fig. 3, that shows the power spectrum and the position of the time segment in the color-color diagram.

^cIndex of power law ($\propto f^\nu$; f is frequency) noise.

^dRMS of power law; lower limit of integration is 0.004 Hz.

^eCentroid frequency of Lorentzian ($\propto \lambda/[(f - f_0)^2 + (\lambda/2)^2]$).

^fFull width at half maximum (FWHM) of Lorentzian.

^gRMS of Lorentzian.

Table 2. Best fit model^a parameters for the $\sim 3.4 - 14$ keV galactic ridge spectrum (*RXTE* PCA) from the position of 1A 1744–361 (when this source was not in outburst).

Model Component	Parameter	value ^b
Absorption	N_{H} (10^{22} cm $^{-2}$)	$2.5^{+3.5}_{-2.5}$
Raymond-Smith	kT (keV)	$1.8^{+0.7}_{-0.3}$
Power law	Photon index	$1.4^{+0.9}_{-0.8}$

^a*wabs(raymond+powerlaw)* model in *XSPEC*.

^bBest fit parameters with 1σ errors. Reduced $\chi^2 = 15.8/21$. Flux = 2.2×10^{-11} ergs cm $^{-2}$ s $^{-1}$ (3.4 – 14 keV).

Table 3. Fitting of high intensity energy spectrum (ObsID 80431-01-02-02; *RXTE* PCA) from 1A 1744-361 with various spectral models of *XSPEC*.

Model no.	Model ^a	χ^2/dof
1	‘ridge’+ <i>wabs</i> * <i>compTT</i>	$\frac{2084.8}{21} = 99.3$
2	‘ridge’+ <i>wabs</i> *(<i>compTT</i> + <i>bbodyrad</i>)	$\frac{764.9}{19} = 40.3^b$
3	‘ridge’+ <i>wabs</i> *(<i>compTT</i> + <i>bbodyrad</i> + <i>gauss</i>)	$\frac{27.37}{16} = 1.7$
4	‘ridge’+ <i>wabs</i> * <i>edge</i> *(<i>compTT</i> + <i>bbodyrad</i> + <i>gauss</i>)	$\frac{8.9}{14} = 0.6^c$

^aThe ‘ridge’ model is the best fit model for galactic ridge spectrum (Table 2), and the parameters are frozen to the best fit values. For the *compTT* model, spherical geometry is chosen.

^bSee Fig. 4.

^cThe probability (calculated from F-test) of the decrease of χ^2/dof by chance from the value of the previous row to the that of the current row is 3.7×10^{-4} .

Table 4. Best fit parameters (with 1σ error) for the *RXTE* PCA energy spectra^a from 1A 1744–361.

Model parameters	1	2	3	4
N_{H}^{b}	$0.10_{-0.00}^{+1.69}$	$0.10_{-0.00}^{+0.42}$	$2.00_{-0.72}^{+0.69}$	$0.51_{-0.41}^{+0.99}$
$E_{\text{edge}}^{\text{c}}$	$8.43_{-0.13}^{+0.30}$	$8.38_{-0.19}^{+0.23}$	$8.68_{-0.32}^{+0.39}$	$7.89_{-0.18}^{+0.20}$
$D_{\text{edge}}^{\text{d}}$	$0.12_{-0.05}^{+0.03}$	$0.07_{-0.03}^{+0.02}$	$0.16_{-0.04}^{+0.04}$	$0.18_{-0.05}^{+0.05}$
T_{C}^{e}	$3.50_{-0.81}^{+2.38}$	$3.41_{-0.45}^{+1.03}$	$4.09_{-0.47}^{+0.87}$	$3.55_{-0.17}^{+0.38}$
$\tau_{\text{C}}^{\text{f}}$	$9.53_{-2.28}^{+1.94}$	$9.11_{-1.55}^{+1.05}$	$11.58_{-1.61}^{+1.40}$	$14.01_{-1.59}^{+0.91}$
T_{BB}^{g}	$1.31_{-0.06}^{+0.03}$	$1.26_{-0.07}^{+0.05}$	–	–
E_{G}^{h}	$5.97_{-0.07}^{+0.09}$	$5.90_{-0.00}^{+0.11}$	–	–
$\sigma_{\text{G}}^{\text{i}}$	$0.62_{-0.26}^{+0.27}$	$0.70_{-0.29}^{+0.11}$	–	–
EW^{j}	117_{-47}^{+75}	131_{-64}^{+51}	–	–
Flux ^k	2.2×10^{-9}	2.1×10^{-9}	3.1×10^{-10}	2.9×10^{-10}
$\frac{\chi^2}{\text{dof}}$	$\frac{8.9}{14}$	$\frac{13.9}{10}$	$\frac{13.1}{19}$	$\frac{11.7}{19}$

^a1: ObsID 80431-01-02-02 (*plus* symbols of panel *d* of Fig. 3); 2: ObsID 80431-01-02-04 (*plus* symbols of panel *c* of Fig. 3); 3: ObsID 90058-04-01-00 (*diamond* symbols of Fig. 2); 4: ObsID 90058-04-02-00 (*cross* symbols of Fig. 2). First two spectra (high intensity) are fitted with ‘ridge’+*wabs***edge**(*compTT*+*bbodyrad*+*gauss*) model of *XSPEC* (‘ridge’ model is described in Table 3), while the last two spectra (low intensity) are fitted with ‘ridge’+*wabs***edge***compTT* model.

^bHydrogen column density (10^{22} cm $^{-2}$) from *wabs* model in *XSPEC*; imposed lower limit is 0.1.

^cThreshold energy (keV) of the edge (*edge* model in *XSPEC*).

^dAbsorption depth at the threshold of the edge.

^eTemperature (keV) of the Comptonizing plasma (*compTT* model in *XSPEC*).

^fOptical depth of the Comptonizing plasma.

^gBlackbody temperature (keV) (*bbbodyrad* model in *XSPEC*).

^hCentroid energy (keV) of Gaussian emission line (*gauss* model in *XSPEC*); imposed lower limit is 5.9.

ⁱWidth (keV) of Gaussian emission line; imposed upper limit is 1.0.

^jThe equivalent width (eV) of Gaussian emission line.

^kFlux in ergs cm⁻² s⁻¹ (3.4 – 14 keV).

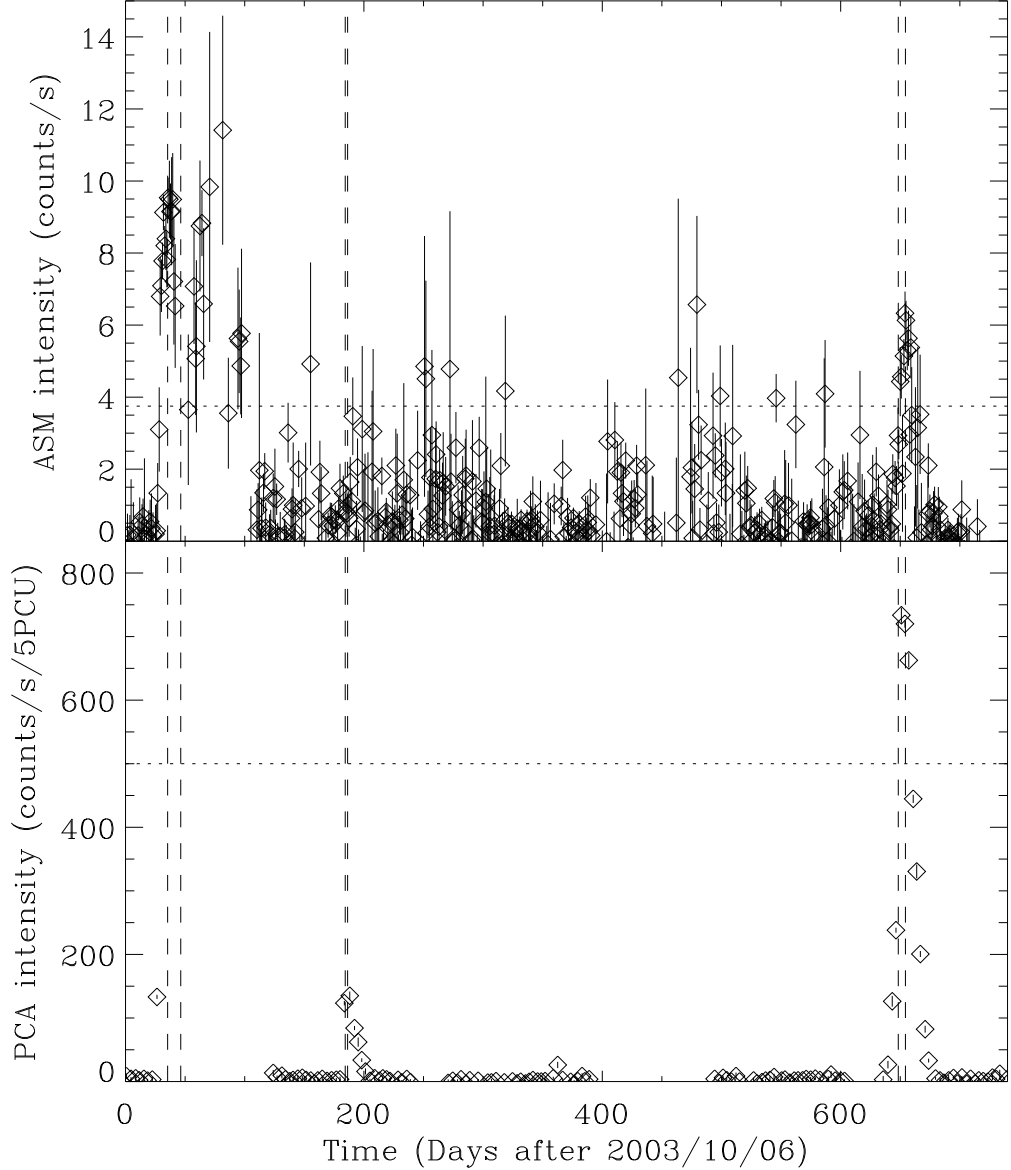


Fig. 1.— The long term ASM and PCA (galactic bulge scan) light curves of 1A 1744–361. The pairs of dashed vertical lines show the time intervals of pointed *RXTE* observations of the source during the outbursts in 2003, 2004 and 2005. Each of these intervals contains several observations. The dotted horizontal lines give the 50 mCrab intensity level. Note that the PCA galactic bulge scan was prevented due to the angular proximity to the sun during the first outburst, which caused a data gap. We also note that 1A 1744–361 was probably not detected with the PCA in the quiescent state, and outburst activity is rare, as the PCA galactic bulge scan did not find any outburst from this source during the years 1998 – 2002.

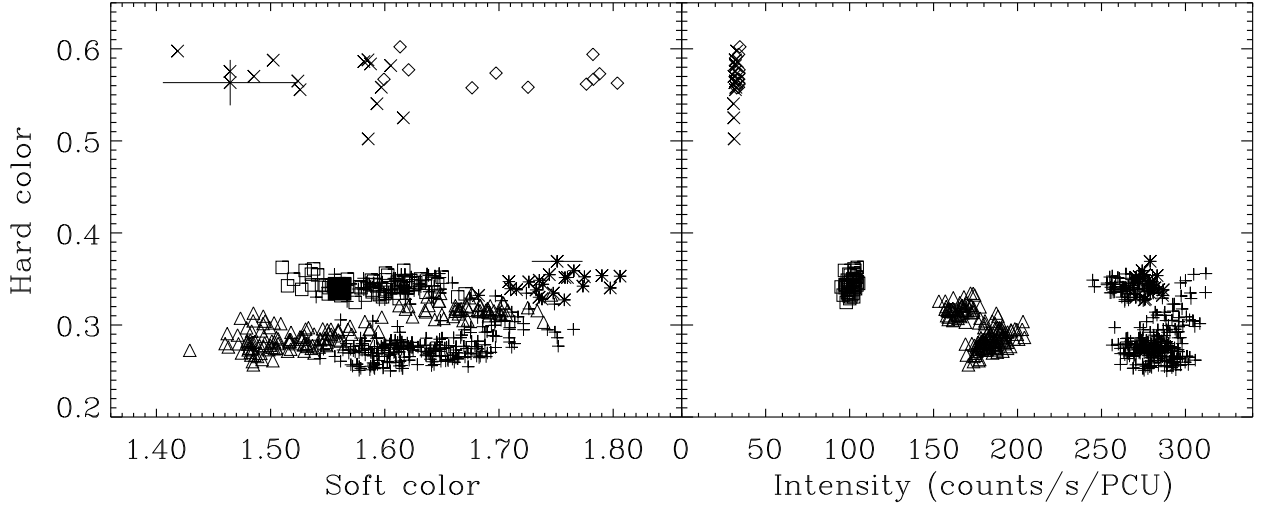


Fig. 2.— Color-color diagram (left panel) and hardness-intensity diagram (right panel) of 1A 1744–361 using the *RXTE* PCA pointed observation data of the years 2003, 2004 and 2005. The definitions of the colors and the energy range of the intensity are given in § 2. Here we use the data only from the top Xenon layers. Each point is for 64 s of data. The *cross* symbols are for the ObsID 90058-04-02-00 (2004 data that show a ~ 2.5 Hz QPO, and a possible kHz QPO (Bhattacharyya et al. 2006)), the *diamond* symbols are for ObsID 90058-04-01-00 (2004 data that show a ~ 3.5 Hz QPO (Bhattacharyya et al. 2006)), the *square* symbols are for the ObsID 91050-05-01-00 (2005 data that show a thermonuclear X-ray burst (Bhattacharyya et al. 2006)), the *triangle* symbols are for the rest of the 2005 data, the *star* symbols are for the two segments of the ObsID 80431-01-02-00 (2003 data that show energy dependent dips (Bhattacharyya et al. 2006); but the dip portions are excluded), and the *plus* symbols are for the rest of the 2003 data. The *filled square* symbol is for the data just before the burst. Here we exclude the time intervals of obvious flares, burst and dips. Two sets (one for low intensity data and another for high intensity data) of typical 1σ error bars are shown in the color-color diagram. The ranges of soft color, hard color and intensity strongly indicate the atoll nature of 1A 1744–361 during the outbursts (see § 2).

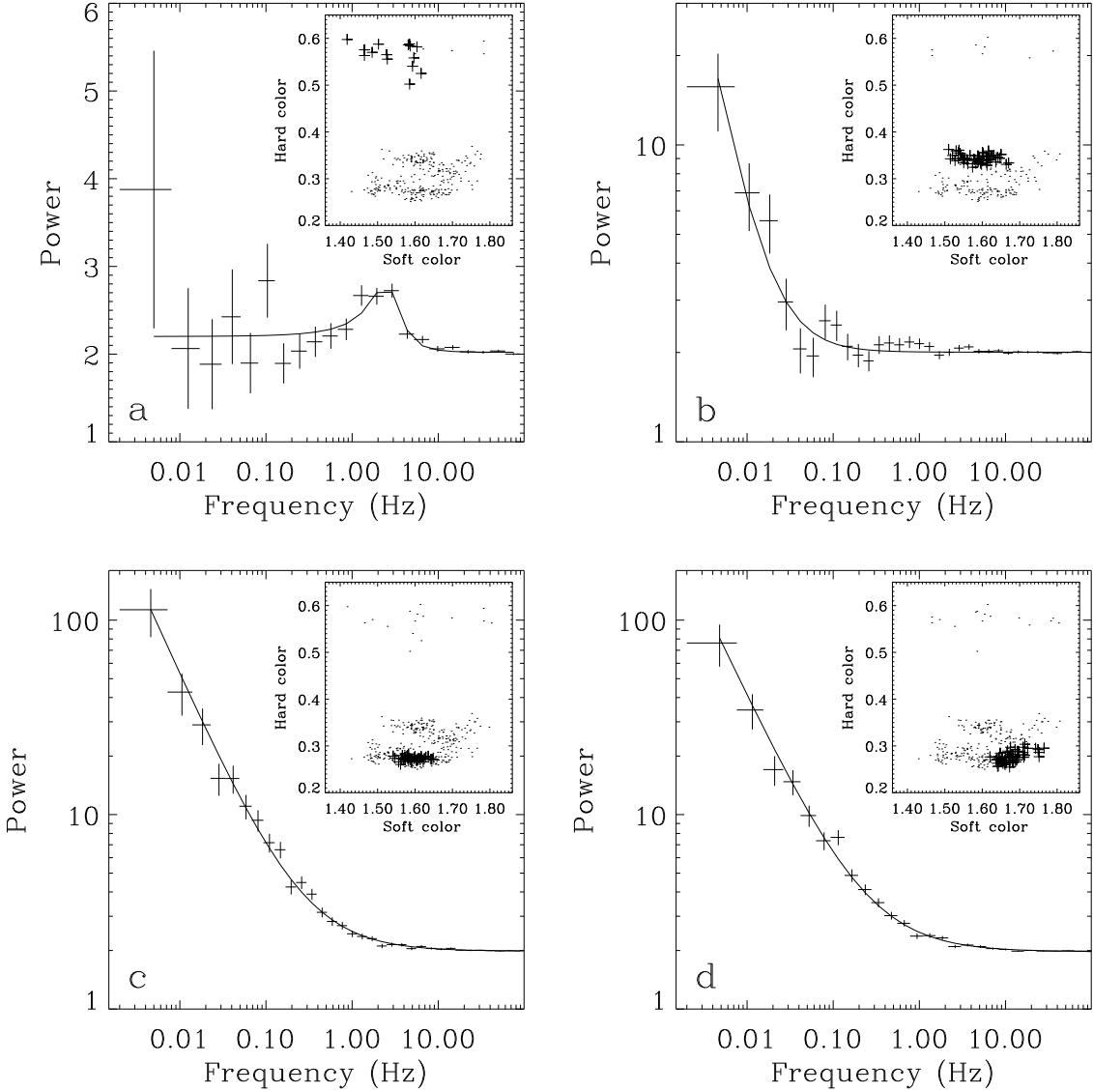


Fig. 3.— Low frequency power spectra (for the energy range $\sim 2.6 - 30$ keV) of 1A 1744-361 using *RXTE* PCA data. Panels *a*, *b*, *c* and *d* are for the ObsIDs 90058-04-02-00, 91050-05-01-00, 80431-01-02-04 and 80431-01-02-02 respectively. For each panel, the main panel shows the data points and the best fit model (solid line; see Table 1). The horizontal lines around the data points give the frequency bin, and the corresponding vertical lines give the 1σ errors of powers. Each inset panel shows the color-color diagram (same as in Fig. 2) and the *plus* symbols show the data used to calculate the power spectrum in the corresponding main panel. Panel *a* is for the low intensity AHB (see § 2) state of the source, and the power spectrum is well fitted with a constant+Lorentzian model. The ‘constant’ describes the Poisson noise level and the Lorentzian describes the dipper QPO (Bhattacharyya et al. 2006). Panels *b*, *c* and *d* are for the banana state of 1A 1744-361, and a constant+powerlaw model fits the power spectra well. Here the ‘powerlaw’ describes the very low frequency noise (VLFN).

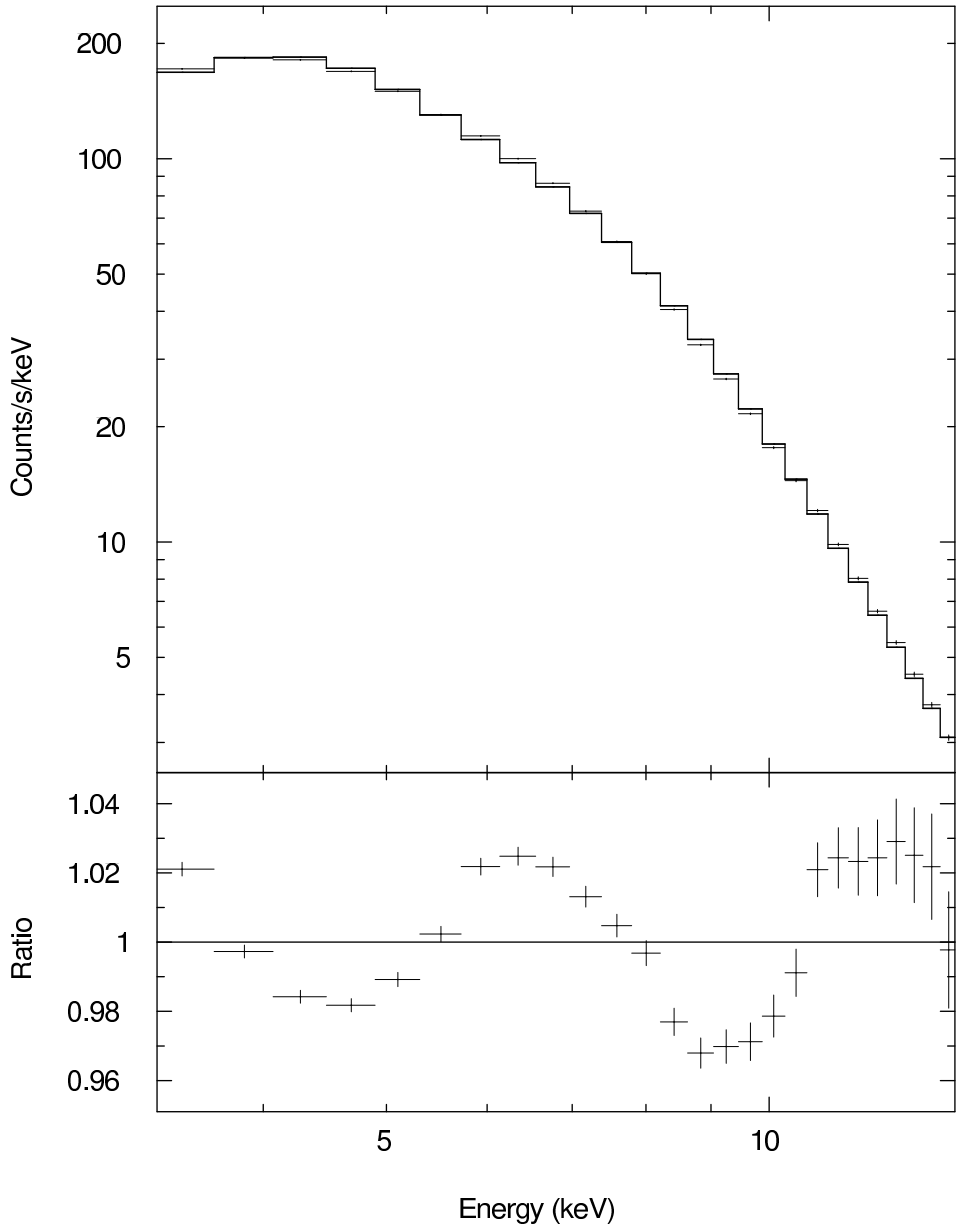


Fig. 4.— *RXTE* PCA energy spectrum from 1A 1744–361 for the ObsID 80431-01-02-02 (time segment denoted by *plus* symbols of the inset panel of panel *d* of Fig. 3; high intensity banana state). Here we use only the top Xenon layers, and fit the data with a continuum model (*'ridge'*+*wabs**(*compTT*+*bbodyrad*) in *XSPEC*; model no. 2 of Table 3). The *'ridge'* model is the best fit model (*wabs**(*raymond*+*powerlaw*) in *XSPEC*) for galactic ridge emission and we fix the parameters of this model to the best fit value (Table 2). The upper panel shows the data points and the model (solid histogram). The lower panel shows the data to model ratio. The lower panel suggests that an additional broad emission line model component (near ~ 6 keV) and an additional absorption edge model component (near ~ 8 keV) are required for a good fit.